International Journal of Environmental Sciences
ISSN: 2229-7359
Vol. 11 No. 6, 2025
https://theaspd.com/index.php

ANN Based Improved Dynamic Set Point Weighted PI Controller in Real Time Experimentation

Pubali Mitra Paul[1], Chanchal Dey[2], Rajanikanta Mudi[3], Parikshit Kumar Paul[4]
[1]Department of Electronics and Communication Engineering, Brainware University, Barasat, 700125, India, ORCID: 0000-0002-8163-144X
pubali.mitra.cu@gmail.com
[2]Instrumentation Engineering, Department of Applied Physics, University of Calcutta, Calcutta, 700009, India, ORCID: 0000-0001-6562-6571, cdaphy@caluniv.ac.in
[3]Department of Instrumentation and Electronics Engineering, Jadavpur University, Calcutta, 700032, India, ORCID: 0000-0001-7097-1812, rajanikanta.mudi@jadavpuruniversity.in
[4]Department of Electronics and Communication Engineering, Swami Vivekananda Institute of Science and Technology, Dakshin Gobindapur, Sonarpur, Kolkata,700145, India, parikshitkrpaul.cu@gmail.com

Abstract *– Artificial Neural Network or ANN, modeled by the neuron structure of the human brain, have the ability to process and interpret complex, non-linear patterns through interconnected layers and activation functions. In this work, a novel control strategy for DC servo positioning systems is proposed by integrating neural network concepts into classical control. Traditional PID controllers, especially without derivative action, face challenges in tuning and exhibit sluggish behavior and noise sensitivity. While dynamic set point weighting (DSW) techniques improve PI controller performance, their design is complex and often unsatisfactory for systems with high open-loop gain. To overcome these limitations, neuron-based improved dynamic set point weighted PI controller (IDSWPI) is introduced. In this approach, the weighting factor is adaptively computed online using a neuron with a sigmoidal activation function based on instantaneous error changes. Simulation and real-time experimental results demonstrate that the proposed IDSWPI controller offers superior performance compared to conventional fixed and dynamic set point weighting methods.*
Keywords *– Artificial Neural Networks (ANN), activation function, Proportional Integral (PI) controller; DC servo motor; fixed set-point weighting; improved dynamic set-point weighting*

1. INTRODUCTION

Artificial Neural Networks (ANNs) mimic the human brain's neuronal architecture, that are capable of processing and transmitting signals while carrying out various activities. Unlike traditional computing systems, which rely heavily on explicit programming and sequential operations, ANNs emulate the brain's ability to learn from experience. The brain exemplifies an energy-efficient and compact system capable of solving complex problems that often lie beyond the capabilities of current computers [1].

The biological brain demonstrates [2] remarkable proficiency in pattern recognition and generalization—abilities that conventional computers struggle to replicate. While computers excel at deterministic tasks such as arithmetic operations and data processing, they face significant challenges in tasks involving perception, adaptation, and prediction.

Research in neuroscience has revealed that the brain encodes and processes information as patterns [3]. This capability enables humans to recognize individual faces from various angles and under different conditions, showcasing the flexibility and robustness of biological learning systems [4]. Inspired by these findings, ANNs store information as interconnected patterns within a network of simple processing elements, or "neurons." Through a process known as training, these networks adjust their internal connections to capture complex relationships in data, allowing them to perform sophisticated tasks such as classification, prediction, and decision-making [5].

A fundamental departure from conventional computing, ANN-based systems rely on massively parallel architectures and adaptive learning mechanisms [6]. Rather than following rigid instructions, they exhibit properties such as self-organization, generalization, learning, and even forgetting—concepts more akin to biological processes than to traditional algorithmic logic.

These biologically inspired computational models are expected to drive significant advancements in the field of artificial intelligence [7]. By enabling systems that can learn and adapt in a human-like manner, ANNs promise more resilient and flexible solutions, particularly under conditions of uncertainty or overload, where conventional systems often fail. A typical structure of neural networks is shown in Fig. 1.

Now, servo mechanisms have wide applications in robotics, machine tools, space and defence pointing, complex motion control systems etc [8]. Majority of servo system employ DC motors with permanent

magnet connected to the load by a transmission chain (or gearbox) and a position sensor is mounted on the motor shaft [9]. By having feedback signal (motor position) either PID control or compensation techniques [10, 11] are being employed to achieve satisfactory performance. In DC servo positioning, inclusion of derivative (D) action in control strategy is a popular choice but it results sluggish response with noise sensitivity. Without incorporating the damping behaviours (D action) suitable tuning of proportional-integral (PI) controller is found to be quite challenging [12-14]. Controlling the position of DC servo motor with conventional PI controller may lead to undesirable oscillations. Hence, to mitigate such limitation numbers of control strategies [15] are being explored by the researchers to ensure satisfactory set point tracking along with efficient load recovery.

Due to model independent feature relay based [16] tuning mechanism is well accepted for initial controller setting [15-19]. However, relay-tuned PI controllers often do not provide satisfactory closed-loop performance for servo processes, as shown in Fig. 2. Both the set point and load recovery responses are oscillatory. To address this limitation, researchers have reported the set point weighting mechanism as one of the well-established methodologies [20-26]. Additionally, set point filtering techniques [27-35] can restrict oscillations during set point tracking but may not offer significant improvement during load variation. The proportional term in the fixed set point weighting case is multiplied by a constant β where $0 < \beta \leq 1$ (usually 0.4 to 0.6) [27]. However, it causes retarded response and hence results relatively large rise time. To overcome this limitation, the author in [28] suggested variable set-point weighting (VSW). In place of using a fixed weighting factor, VSW utilizes different weighting factors during three different phases of set point tracking to limit the initial overshoot sacrificing the rise time. The set-point weighting for model predictive control is documented in [30]. In [31], the weighting factor is obtained for unstable processes with zero by optimizing the value of integral square error (ISE) of the controlled variable. However, it fails to provide any improvement in process response in load recovery. To find out the optimal value of the weighting factor various optimization techniques are being employed in [32]. In [33] the set-point weighting is applied to direct synthesis based PID controller in order to provide a better closed-loop response for integrating processes. In [34], it uses a modified Smith predictor with the weighted set points for different integrating processes/long delay time systems. In [35], an augmented set point weighted PI controller is developed for nonlinear processes.

Finally, researchers are also looking at how the knowledge of experienced process operators can be incorporated into a weighted fuzzy logic-designed set point structure for PID controller and choice weight factor [36, 37]. The weighting factor in this case is generated by the a priori fuzzy rule set for instantaneous process error and rate of change of error. Dynamic set point weighting - This work in [38] and the PI controller variant of PID controllers respectively, both balance servo phases as well as regulatory ones. Similar schemes are tried in [40, 41] and real-time test is done on DC servo position control systems.

From the prior reported set point weighting schemes, it is quite evident that fixed set point weighting causes sluggish behaviour and fails to provide any improvement during load change. Sluggishness during set point tracking is augmented by variable set point weighting (VSW) scheme but it turns out to be ineffective during load recovery. In contrast, the dynamic set point weighting (DSW) method has the capability to progress enhance performance in both the regulatory and servo phases. However, the DSW tuning mechanism is not quite straight forward for realization and found to be less effective for dead time-based integrating processes. Hence, to mitigate such limitation an improved dynamic set-point weighting (IDSW) technique is reported here. The weighting factor is intended from neural network structure. Here, the neural network is designed with logistic function or non-linear sigmoid activation function as input with the instant process change of error. Mainly, the non-linear activation function allows backpropagation that can predict better weighting factor on the basis of neurons. In the case of IDSW the control strategy using NN based non-linear activation function can be described as – during closed loop operation as the process output is approaching quickly towards the set point, proportional action gets weakened to avoid possible large overshoot or undershoot. Alternatively, as the process exhibits a rapid departure from the set point, the proportional control action is intensified to mitigate and limit the deviation effectively. Such suitable variation in proportional action is found to be quite effective during closed-loop operation irrespective of servo and load regulation phases.

Efficacy of the proposed IDSW technique with PI controller (IDSWPI) is evaluated on DC servo motor. Supremacy of IDSWPI is ascertained through closed loop performance analysis in comparison with the PI controller using fixed set point weighting (FSWPI) and dynamic set point weighted PI controller (DSWPI). For quantitative performance estimation performance indices – percentage overshoot (%OS),

rise time (t_r), settling time (t_s), integral absolute error (IAE), integral time absolute error (ITAE), and total variation (TV) in control action are assessed for each condition separately. Furthermore, noise sensitivity of IDSWPI is examined in presence of measurement noise. Relative stability margins are also calculated in terms of gain margins (GM) and phase margins (PM) values.

Designing of the proposed IDSWPI controller in detail is reported in the subsequent section 2. Section 3 describes the performance and stability analysis of the reported scheme along with FSWPI and DSWPI controllers on two separate servo position control setups in real time along with their simulation models. Conclusion is provided at the end in section 4.

2. Design of IDSWPI controller

A comprehensive block diagram of the suggested IDSWPI controller is depicted in Figure 3, illustrating the dynamic weighting factor. (β_f) is determined using an ANN model that comprises with a straightforward activation function based on change of error (Δe) as input layer in each sample instant, as indicated by the dotted boundary (Fig. 3).

2.1 Realization of IDSWPI controller

The discrete implementation of the conventional PI controller at sample instant k is expressed as:

$$u(k) = k_c\left[e(k) + \frac{\Delta t}{T_i}\sum_{j=0}^{k} e(j)\right]. \quad (1)$$

k_c is termed as proportional gain, T_i is integral time, Δt is the sampling interval and $e(k)$ is the error at k^{th} instant. Error at k^{th} instant is given by $e(k) = y_r - y(k)$ where y_r is the set value and $y(k)$ is the output of process at k^{th} instant. The values of k_c and T_i are considered on the basis of ultimate cycle-based tuning [15-19] equations as given by Eqns. (2) and (3).

$$k_c = 0.45K_u, \quad (2)$$

$$T_i = \frac{T_u}{1.2}. \quad (3)$$

Here, K_u and T_u are considered as ultimate gain and ultimate period respectively that are generally observed by relay feedback method [19]. In the proposed IDSWPI controller, a variable weighing factor is presented alongside the proportional term of the PI controller, leading to the expression given by Eqn. (4).

$$\begin{aligned} u(k) &= k_c\left[\{\beta_f\, y_r - y(k)\} + \frac{\Delta t}{T_i}\sum_{j=0}^{k} e(j)\right] \quad (4)\\ &= k_c\left[\{y_f - y(k)\} + \frac{\Delta t}{T_i}\sum_{j=0}^{k} e(j)\right]. \end{aligned}$$

In Eqn. (4), β_f is the dynamic weighting factor calculated from an activation function of a single neuron. The nature of the activation function is considered to be sigmoid function as shown in the Fig. 5.

A. ACTIVATION FUNCTION

As demonstrated, an activation function in an artificial neural network model uses the inputs of a neuron to determine its output as shown in Fig. 4. It gives the network non-linearity, which is crucial for allowing the model to learn and represent intricate designs and connections in information. Sigmoid is an effective and widespread activation function that can be used in different cases. Sigmoid activation function interprets the range of the input layer from $(-1, +1)$ to the output range as [0,1]. Eqn. (5) provides the mathematical relation of the sigmoid shaped activation function where the weighting factor is examined from the instant value of the change of error (Δe). Time derivative of the specified sigmoid function of a single neuron is always greater than zero which signifies that it is a smoothly increasing monotonic function.

$$\beta_f = \frac{1}{1 + e^{-(\alpha \times \Delta e)}}. \quad (5)$$

Eqn. (5) uses Δe as the change of error and α (>0) as the sigmoid function's slope parameter.

At k^{th} sampling instant $\Delta e(k)$ is defined by Eqn. (6). Fig. 5. shows the nature of sigmoid function where α determines the slope of the function at origin. Here, we have introduced sigmoid function to find out the optimum weighting factor based on deep neural network.

$$\Delta e(k) = e(k) - e(k-1) \quad (6)$$

From Eqn. (5) it is clear that the slope of the activation function varies continuously depending on the instantaneous value of Δe based on neural network structure. The nature of weighting factor β_f over the normalized variation of Δe (-1, +1) is shown in Fig. 5. Here, the choice of α is very crucial as it dictates the desired variation of β_f .

From Eqn. (4), the control law of the proposed IDSWPI controller is given by

$$u(s) = k_c\left[\{\beta_f\, y_r(s) - y(s)\} + \frac{1}{T_i s}\,(y_r(s) - y(s))\right]. \quad (7)$$

2.2 Control Strategy of the proposed IDSWPI controller

The representative tracking response of a DC servo motor and the associated variation of the weighting factor $(\beta_f\ )$ are depicted in Fig. 6. Here, the proportional component of the PI controller is modified by continually varying β_f on the process operating conditions i.e., the change of error that in sequence modify the component of the proportional term of the PI controller. For a clear and thorough comprehension of proposed technique during transient phases, two distinct operating points are chosen and the corresponding weighting factor $(\beta_f\ )$ values are discussed subsequently –

(i) For the operating point 'A' (Fig. 6) where process output is far below the set point $(i.e.\, y < y_r\ )$ and moving towards the set point, the value of Δe is large and negative. Hence, the weighting factor (β_f) associated with the proportional term must be smaller and here it is found to be $0 < \beta_f < 0.5$. Thus, the resulting control action of the proposed IDSWPI controller is minimized and hence it results retard the system responsiveness so that the possible large overshoot may be avoided.

(ii) For the operating point 'B' (Fig. 6.), the output of the process is approaching towards the set value from some higher value $(i.e.\, y > y_r)$, it results Δe to be positive. Hence, the resulting value of the weighting factor is found to be high $1 > \beta_f > 0.5$. Such larger value of β_f would help to exhibit superior closed loop response by restricting the possible under shoot.

Thus, it is clear from the previous discussions that the dynamic set point modifier β_f can provide the required variation in the control action to limit the process oscillations around the set value and improve the transient responsiveness.

3. Performance analysis of the proposed IDSWPI controller

Structure of the mentioned IDSWPI controller is substantiated with the real time experimentation along with simulation study of the respective servo process model. The proposed IDSWPI controller is evaluated along with two well-established set point weighting PI control schemes i.e. fixed set point weighting (FSWPI [27]) and dynamic set point weighting (DSWPI [38]). For easy and effective comparison, the matching performance indices – %OS, t_r, t_s, IAE, ITAE and TV are assessed independently for every configuration.

3.1 Experimentation with Quanser - QUBE

Quanser [42] uses a PC-based QUBE Servo, a small direct-drive rotary servo unit with built-in DAQ, to test the suggested IDSWPI controller's performance in a variety of DC servo control tests. Fig. 7 displays the schematic diagram of its motor armature circuit, and Table 1 lists the relevant mechanical and electrical data.

The disc load itself has a moment of inertia represented by J_d, whereas the motor shaft connects to the load hub, which is used to attach the disc with a moment of inertia J_h.

The back-emf $e_b(t)$ is dependent on the speed of the motor shaft ω_m, and the back-emf constant is k_m. The source of back-emf is given by

$$e_b(t) = k_m \omega_m(t). \quad (8)$$

Using Kirchoff's Voltage Law, one can write the following relation

$$v_m(t) - R_m\, i_m(t) - L_m \frac{di_m(t)}{dt} - k_m \omega_m(t) = 0. \quad (9)$$

Since the motor inductance L_m is much lesser compared to its circuit resistance, it can be ignored. Hence, the Eqn. (9) can be written as

$$v_m(t) - R_m\, i_m(t) - k_m \omega_m(t) = 0. \quad (10)$$

Solving for $i_m(t)$, the motor current is calculated as

$$i_m(t) = \frac{v_m(t) - k_m \omega_m(t)}{R_m}. \quad (11)$$

Now, solving the prior equations with given parameters (Table 1), one can get the open loop transfer function of the DC motor-based position control system as given by

$$G_\theta(s) = \frac{26.5\, e^{-0.01s}}{s(0.155s+1)}. \quad (12)$$

Here, the QFLEX 2 modules are used to configure the QUBE Servo during experimentation. The 18V brushed DC motor drives a readily attachable inertia (0.6 × 10−6 kg-m2) disc. A rotary encoder measures

the disc's angular position and the motor's angular speed (2048 lines/revolution). The encoders and motor are connected to the built-in DAQ block's encoder input (EI).

The block diagram depicting connections between various system components of the QUBE Servo is observable in Fig. 8, while Fig. 9 displays a snapshot of the QUBE Servo with the inertial disc module. The experimental setup in the laboratory is shown in Fig. 10. The power amplifier in charge of managing the DC motor is connected to the Analog Output (AO) channel. The integrated PWM amplifier is connected to the DAQ Analog Input (AI) channel. The DAQ uses QFLEX 2 to link with the PC via a USB connection.

The usefulness of the mentioned IDSWPI controller for the QUBE Servo system is assessed through both simulation and real-time experimentation. Figure 11 illustrates the simulation responses and the control actions of all reported controllers, including the proposed IDSWPI controller, during set point tracking and load rejection. Performance indices for these responses are detailed in Table 2. From the simulation results it is evident, that the initial overshoot is amazingly minimized in case of proposed IDSWPI controller in comparison with FSWPI and DSWPI controllers. Lower settling time with no oscillation substantiate the improved behaviour of the proposed controller (IDSWPI) with comparable rise time of the other controllers (FSWPI and DSWPI). Reduced values of IAE, ITAE and TV clearly establish the superior performance of the proposed IDSWPI controller.

Additionally, in the simulation study, the improved performance of the proposed controller is also verified in real-time, further supporting the effectiveness of the IDSWPI controller compared to FSWPI and DSWPI schemes. Real-time responses, including control actions for DSWPI and the proposed IDSWPI controllers, are shown in Fig. 12, whereas FSWPI exhibits failure due to significant oscillations. The superiority of the IDSWPI controller is also confirmed by the performance indices listed in Table 2. Similar to the simulation study, it is noted that the IDSWPI controller effectively eliminates the initial overshoot, and the IAE, ITAE, and TV values are significantly lower compared to other reported PI controllers with weighting mechanisms (DSWPI, FSWPI). Noise sensitivity of proposed controller in comparison to DSWPI is also evaluated during their closed loop operation in presence of measurement noise (with power 0.001) as represented in Fig. 13. It obviously substantiates that the suggested IDSWPI controller has relatively strong noise immunity.

3.2 Experimentation with Quanser - DCMCT

The DCMCT is a well-regarded DC servo position control experimental setup developed by Quanser [43]. It involves attaching a load to an encoder. The DCMCT hardware consists of an analog tachometer signal, a servo potentiometer for measuring load angle, a breadboard for implementing analog controllers, and analog-to-digital converters (ADCs). This experimental setup is associated to a PC via USB connectors, as depicted in Figs. 14 and 15. The open-loop transfer function of the DCMCT motor for position control is given by:

$$G_\theta(s) = \frac{19.9e^{-0.01s}}{s(0.09s+1)}. \quad (13)$$

During the simulation study, the response of the proposed IDSWPI controller is evaluated in comparison with FSWPI and DSWPI controllers, as shown in Fig. 16. The graphical responses specify that the proposed controller demonstrates significantly improved performance with minimal overshoot and shorter settling time compared to the other two controllers (FSWPI and DSWPI). Performance indices including IAE, ITAE, and TV values in Table 3 show that the IDSWPI controller outperforms the FSWPI and DSWPI controllers.

In addition to the simulation study, the performance of the proposed IDSWPI controller is also assessed in real-time experimentation alongside other established controllers (DSWPI, FSWPI) using DCMCT, as illustrated in Fig. 17.

Associated performance indices are provided in Table 3. Due to unbounded oscillations, responses for FSWPI controller are not included in the Fig. 17. DSWPI settings provide large oscillations and higher IAE, ITAE and TV values whereas IDSWPI controller offers lesser overshoot and lower settling time. The IDSWPI response is relatively sluggish than DSWPI controller resulting minor increase in rise time value. From the responses obtained during both simulation and practical experimentation the proposed IDSWPI controller is found to be superior to the other reported controllers (DSWPI, FSWPI) in the same category.

3.3 Selection of slope parameter (α)

In Eqn. (14), α is the slope curve parameter of the sigmoid shaped activation function which is required to be chosen judiciously. Appropriate choice of α can provide the desired response by the proposed controller. Based on extensive simulation experimentations the value of α is selected as 25 for the proposed scheme. The characteristics of variation of IAE, ITAE and TV values for different values of α are studied for the reported servo processes (QUBE and DCMCT) and the corresponding variation of α is shown in the Figs. 18 and 19. However, the choice of α is to be adjusted with the time constant value of the concerned processes. Here, it is to mention that the IAE, ITAE and TV values with varying α are found to be least for $\alpha = 25$ and the corresponding nature of variations for both QUBE and DCMCT process model are also shown in Figs. 20, 21 and Figs. 22, 23 respectively. This particular slope $(\alpha = 25)$ of the activation function is chosen for entire simulation and real-time experimentation with the proposed IDSWPI controller.

4. Stability analysis

The proposed IDSWPI controller is nonlinear in nature and hence to offer a straight forward stability analysis of the proposed controller is a difficult task. So, towards achieving relative stability margins, Gain Margin (GM) and Phase Margin (PM) values are calculated for each processes at the two extreme boundary values of β_f . Here, during closed loop operation we consider the maximum value of β_f ($\beta_{f\,max}$) as well as the minimum value of β_f ($\beta_{f\,min}$) for all the reported controllers (FSWPI, DSWPI, and IDSWPI) are shown in Figs. 24, 25 and Figs. 26, 27 respectively. Corresponding GM and PM values are calculated (Table 4) with QUBE and DCMCT process models. We also measure the value of maximum sensitivity (Ms) of the proposed IDSWPI controller along with FSWPI and DSWPI settings. It is found that the proposed IDSWPI controller provides more acceptable closed loop stability margins in terms of GM and PM and Ms values as mentioned in Table 4.

5. CONCLUSION

In the above work, a modest and efficient set point weighting method is presented for PI controller. The dynamic weighting factor is a scalar whose value at any time t is computed by the neural network structure based activation function, which lives inside of neuron. The instant change of error during the process and it will give you a simple relationship in weightage factor so this activation function is designed properly the performance of the method has shown in both simulated and two experimental DC servo position control systems at real-time operation. The results have been outstanding in performance and this dynamic weighting scheme seems to be much better than the other set-point methods reported before. The results of the simulation demonstrate how resilient the suggested method is to a large range in process time delay.

On the basis of stability analysis, it is clear that the suggested controller exhibits greater stability across a wide range of operating parameters. Its simplicity and independence from specific models may allow for the implementation of this method in both higher order linear and nonlinear processes.

REFERENCES

[1] C. K. Chui and X. Li, "Approximation by ridge functions and neural networks with one hidden layer," Journal of Approximation Theory, vol. 70, pp. 131–141, 1992.
[2] G. Cybenko, "Approximation by superpositions of a sigmoidal function," Mathematics of Control, Signals, and Systems, vol. 2, pp. 303–314, 1989.
[3] K.-I. Funahashi, "On the approximate realization of continuous mappings by neural networks," Neural Networks, vol. 2, pp. 183–192, 1989.
[4] P. Ramachandran, B. Zoph, and Q. V. Le, "Searching for Activation Functions," https://doi.org/10.48550/arXiv.1710.05941.
[5] J. Pennington, S. S. Schoenholz, and S. Ganguli, "Resurrecting the sigmoid in deep learning through dynamical isometry: theory and practice," https://doi.org/10.48550/arXiv.1711.04735.
[6] M. Tanaka, "Weighted Sigmoid Gate Unit for an Activation Function of Deep Neural Network," Pattern Recognition Letters, vol. 135, 2020, pp. 354-359.
[7] S. Hayou, A. Doucet, and J. Rousseau, "On the Impact of the Activation Function on Deep Neural Networks Training," 2019, DOI: 10.48550/arXiv.1902.06853
[8] F. G. Shinsky, Process control systems–applications, design, and tuning. NewYork: McGraw-Hill, 1998.
[9] C. Bissel, Control Engineering. NewYork:ChapmanandHall , 1994.
[10]D. E. Seborg, T. F. Edgar, and D. A. Mellichamp, 'Process dynamics and control,' 2nd ed. (New York: Wiley, 2004).
[11]K. Ogata, Modern Control Engineering, Prentice-Hall, New Jersy, 2002.
[12]U. Mondal, A. Sengupta and R. R. Pathak, "Servomechanism for periodic reference input: Discrete wavelet transform-based repetitive controller," Transactions of the Institute of Measurement and Control, vol. 38, no. 1, pp. 14-22, 2016.

[13]H. X. Wu, Z. Y. Qi, J. G. Zheng, and S. M. Zhou, "Back-emf Position Detection Technology for Brushless DC Motor," Applied Mechanics and Materials, vol. 492, 2014, pp. 49-55.
[14]X. Wang, "Modeling and control of a torque load system with servo actuator's dynamics," Proceedings of the Institution of Mechanical Engineers, Part G: Journal of Aerospace Engineering, vol. 231, no. 9, 2017, pp. 1676-1685.
[15]A. O'Dwyer, 'Hand book of PI and PID Controller Tuning Rules,' Imperial College Press, London, 2003.
[16]J. G. Ziegler and N. B. Nichols, 'Optimum setting for automatic controllers,' ASME Transactions, vol. 64, no. 11, pp. 759-768, 1942.
[17]K. J. Astrom and T. Hagglund, 'The future of PID control,' Control Engineering Practice, vol. 9, no. 11, pp. 1163-1175, 2001.
[18]K. J. Åstrom and T. Hagglund, "Revisiting the Ziegler–Nichols step response method for PID control," J. Process Control, vol. 14, no. 6, pp. 635-50, 2004.
[19]K. J. Åstrom and T. Hagglund, "Revisiting the Ziegler–Nichols tuning rules for PI control," Asian J. Control, vol. 4, no. 4, pp. 364-80, 2002.
[20]R. K. Mudi, C. Dey, T. T. Lee, "An improved auto-tuning scheme for PI controllers," ISATrans., vol. 47, no. 1, pp. 45-52, 2008.
[21]C. Dey and R. K. Mudi, "An improved auto-tuning scheme for PID controllers," ISA Transactions, vol. 48, no. 4, pp. 396-409, 2009.
[22]J. C. Basilio, S. R. Matos, "Design of PI and PID controllers with transient performance specification," IEEE Trans. Education, vol. 45, no. 4, pp. 364–70, 2002.
[23]B. D. Tyreus, W. L. Luyben, "Tuning PI controllers for integrator/dead-time processes," Ind. Eng. Chem. Res., vol. 31, no. 11, pp. 2625–8, 1992.
[24]F. Mnif, "New tuning rules of PI-like controllers with transient performances for monotonic time-delay systems," ISATrans., vol. 47, no. 4, pp. 401-6, 2008.
[25]A. Leva, "Autotuning process controller with improved load disturbance rejection," J. Process Control, vol. 15, no. 2, pp. 223-34, 2005.
[26]B. W. Bequette, Process Control Modeling, Design, and Simulation, Pearson Education, New Jersey, 2003.
[27]K. J. Åstrom, C. C. Hang, P. Persson, and W. K. Ho, "Towards intelligent PID control," Automatica, vol. 28, no. 1, pp. 1-9, 1992.
[28]C. C. Hang and L. Cao, "Improvement of transient response by means of variable set point weighting," IEEE Trans. Ind. Electron., vol. 43, no. 4, pp. 477-484, 1996.
[29]M. Chidambaram, "Set-point weighted PI/PID controllers," Chem. Eng. Comm., vol. 179, no. 1, pp. 1-13, 2000.
[30]G. P. Rangaiah, P. R. Krishnaswamy, "Set-point weighting for simplified model predictive control," Chem. Eng. Journal, vol. 50, no. 3, pp. 159-63, 1992.
[31]P. Sree and M. Chidambaram, "Simple method of calculating set-point weighting parameter for unstable systems with a zero," Comp. & Chem. Eng., vol. 28, no. 11, pp. 2433–7, 2004.
[32]R. P. Sree, M. Chidambaram, "Set-point weighted PID controllers for unstable systems," Chem. Eng. Comm., vol. 192, no. 1, pp. 1-13, 2005.
[33]A. S. Rao, V. S. R. Rao, M. Chidambaram, "Direct synthesis-based controller design for integrating processes with time delay," J Franklin Institute, vol. 346, no. 1, pp. 38-56, 2009.
[34]A. S. Rao, V. S. R. Rao, M. Chidambaram, "Set-point weighted modified Smith predictor for integrating and double integrating processes with time delay," ISA Trans., vol. 46, no. 1, pp. 59-71, 2007.
[35]R. J. Mantz, "A PI controller with Dynamic Set-Point Weighting for Nonlinear Processes," IFAC Conference on Advances in PID Control, PID'12, Brescia (Italy), 2012.
[36]A. Visioli, "Fuzzy logic based set-point weight tuning of PID controllers," IEEE Trans Sys Man Cyb, vol. 29, no. 6, pp. 587-592, 1999.
[37]Y. Yang, A. Luo, K. E. Rydberg, "PI control based on fuzzy set-point weighting tracking for hydraulic crane boom system," J. Control Theory and App, vol. 4, no. 4, pp. 327–30, 2006.
[38]R. K. Mudi, C. Dey, "Performance improvement of PI controllers through dynamic set point weighting," ISA Trans., vol. 50, no. 2, pp. 220-230, 2011.
[39]C. Dey, R. K. Mudi, T. T. Lee, "Dynamic set point weighted PID controller," Control and Intell. Syst., vol. 37, no. 4, pp. 212-219, 2010.
[40]P. Mitra, C. Dey, R. K. Mudi, "An Improved Dynamic Set Point Weighted PI Controller for Servo Position Control Application," Proc. IEEE, Second Int. Conf. on Comput. Intell. and Networks, 2016, pp. 145-149.
[41]P. Mitra (Paul), C. Dey, R. K. Mudi, "An Online Dynamic Set Point Weighting Scheme for PID Controller," Proc. IEEE Students' Technology Symposium, 2014, pp. 188-192.
[42]Documentation for the Quanser Qube Servo 2, Canada: Quanser, 2010.
[43]Documentation for the Quanser DCMCT, Canada: Quanser, 2010.

International Journal of Environmental Sciences
ISSN: 2229-7359
Vol. 11 No. 6, 2025
https://theaspd.com/index.php

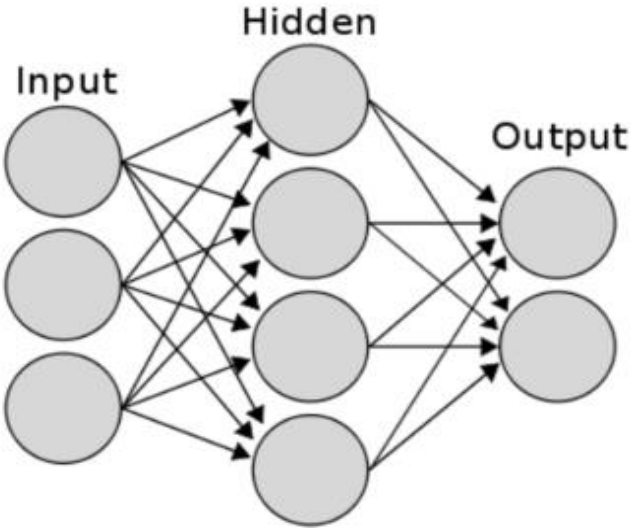

Figure 1. A typical structure of neural network

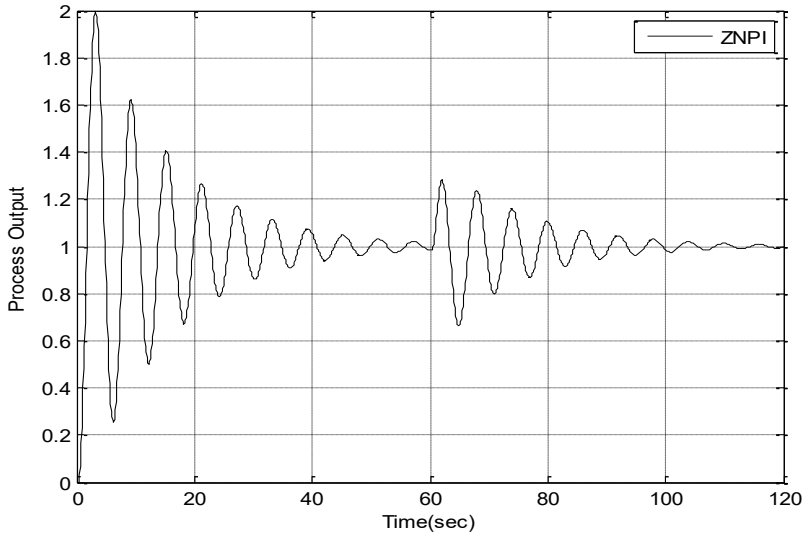

Figure 2. Response for second order process with dead time under ZNPI

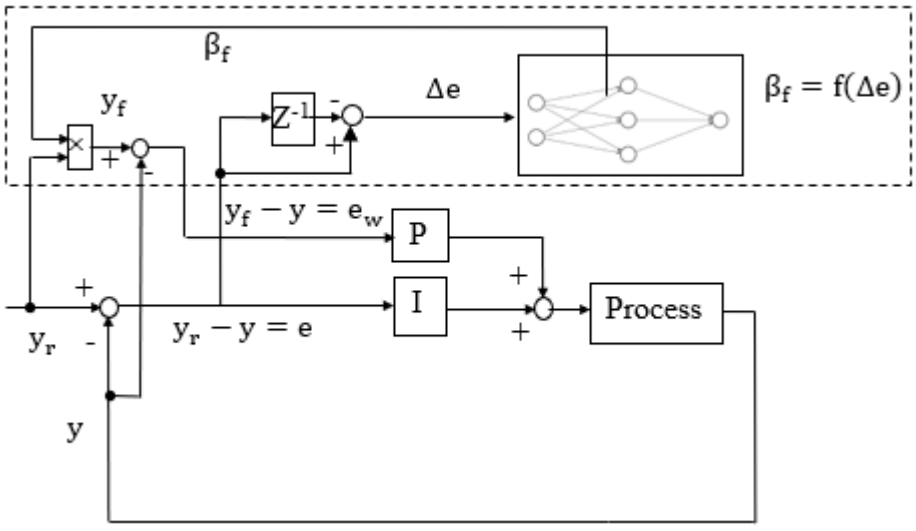

Figure 3. Block diagram of close loop control with IDSWPI controller

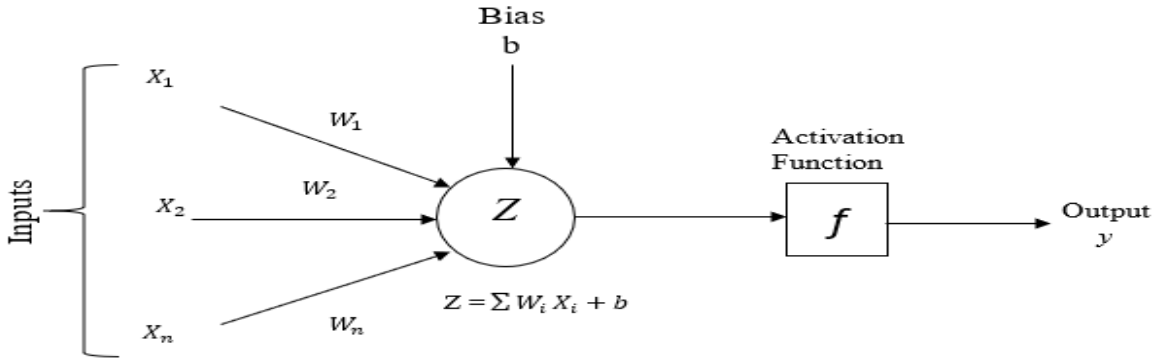

Figure 4. Activation functions in neural networks

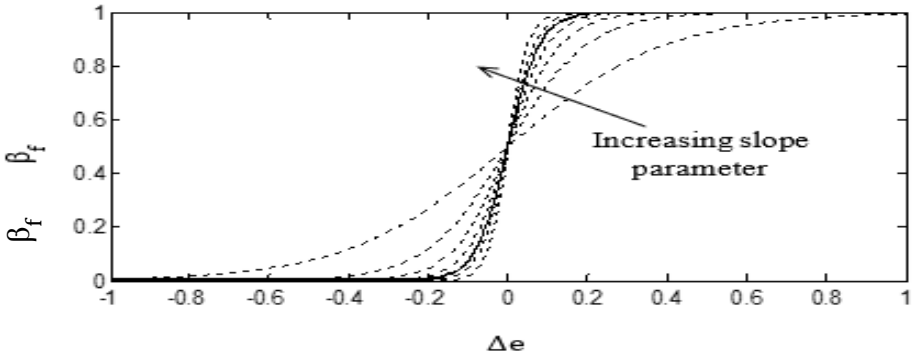

Figure 5. Nature of sigmoid activation function provides weighting factor (β_f) with the input as change of error (Δe)

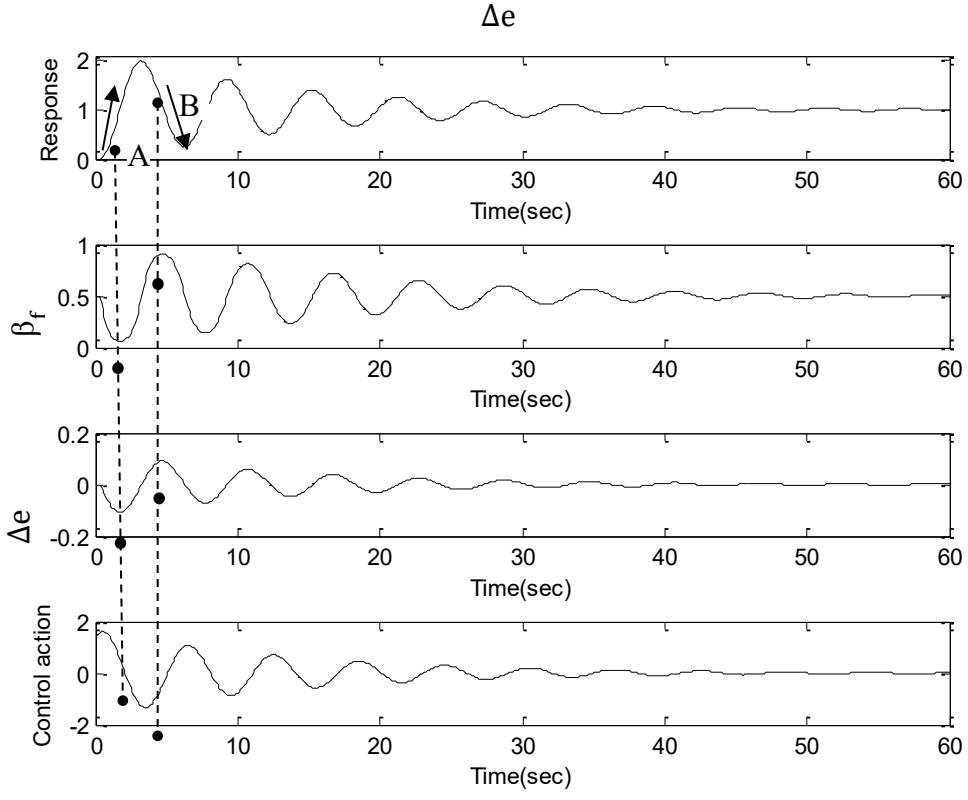

Figure 6. Typical transient response of a servo system.

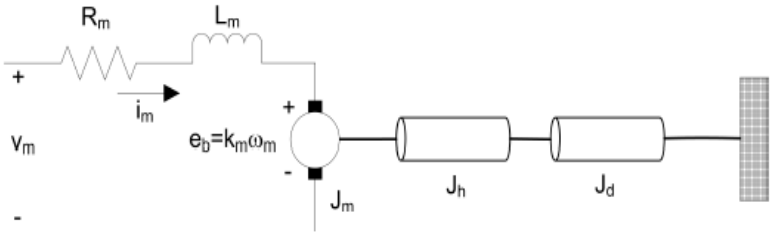

Figure 7. Circuit diagram of QUBE servo DC motor with load

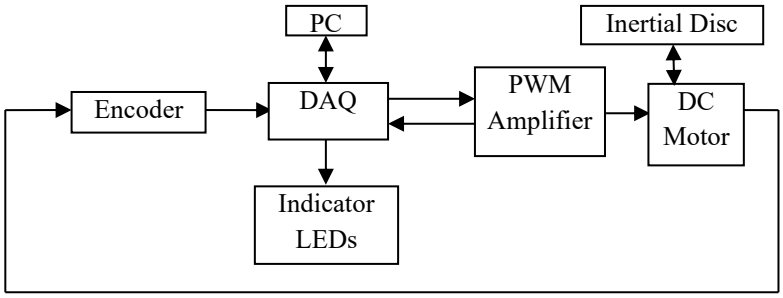

Figure 8. Block schematic for experimental setup of Quanser QUBE servo

Table 1 QUBE servo System Parameters

Symbol		Description	Value
DC Motor	R_m	Terminal resistance	6.3 Ω
	k_m	Motor back-emf constant	0.036 V/(rad/s)
	J_m	Rotor inertia	4×10^{-6} kg – m^2
	L_m	Rotor inductance	0.85 mH
	m_h	Load hub mass	0.0087 kg
	r_h	Load hub mass	0.0111 m
	J_h	Load hub inertia	1.07×10^{-6} kg – m^2
Load Disc	m_h	Mass of disc load	0.054 kg
	r_h	Radius of disc load	0.0248 m

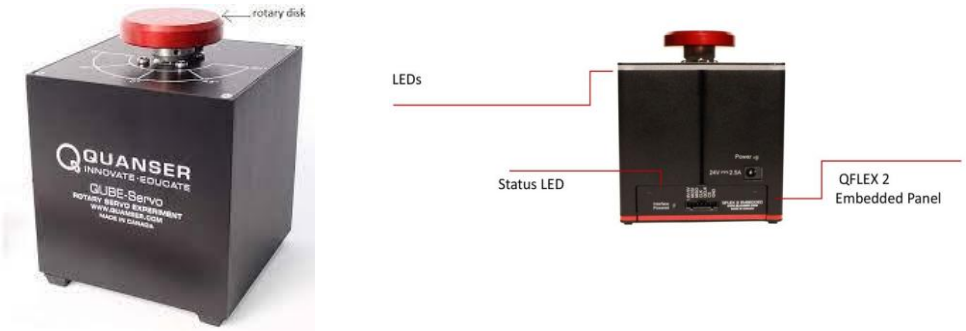

Figure 9. QUBE servo with inertial disc module

Figure 10. Snapshot of experimental setup of Quanser make QUBE servo

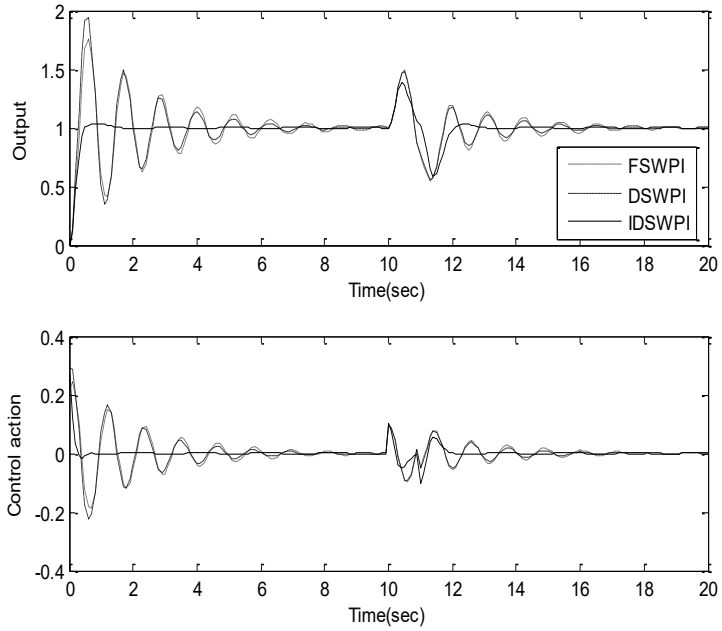

Figure 11. Responses and control actions for QUBE servo system (12) during simulation

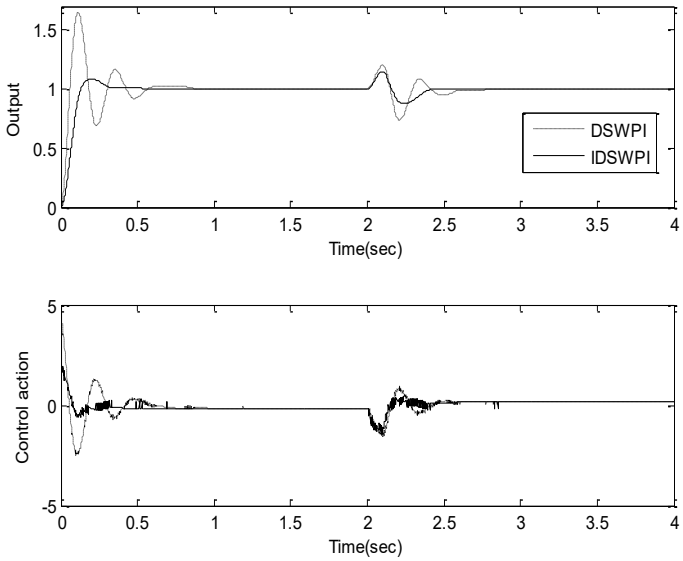

Figure 12. Responses and control actions for QUBE servo system (12) during real time experimentation

Table 2 Performance analysis for QUBE servo system in (12)

		%OS	t_r (sec)	t_s (sec)	IAE	ITAE	TV
FSWPI	simulation	76.2	0.3	10.0	2.4	13.39	0.34
DSWPI		93.5	0.3	10.0	2.2	11.25	0.32
IDSWPI		3.3	0.5	2.6	0.73	4.85	0.12
FSWPI	real time setup	Large oscillation present					
DSWPI		64.7	0.06	1.00	0.19	0.16	0.28
IDSWPI		8.9	0.15	0.55	0.12	0.08	0.25

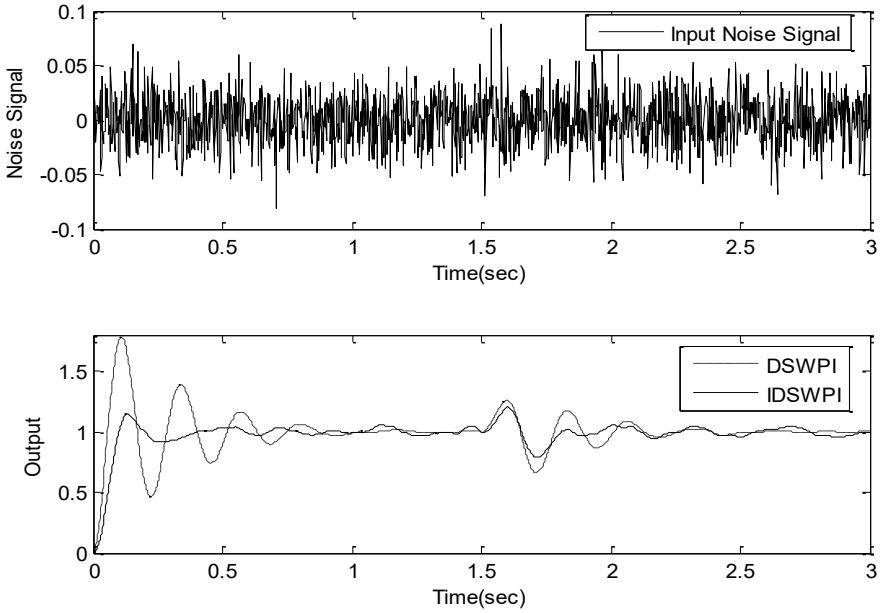

Figure 13. Responses of Quanser QUBE servo for DSWPI and IDSWPI along with noise signal

Figure 14. DC Motor Control Trainer experimental set up

Figure 15. Entire experimental setup of Quenser DCMCT

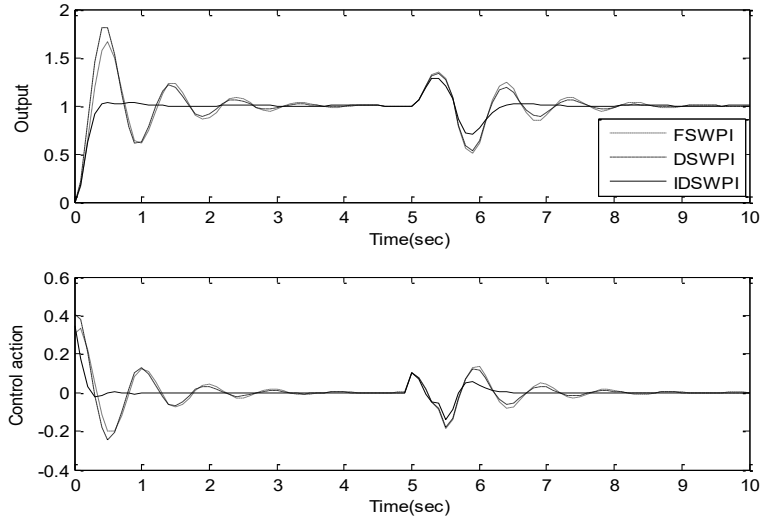

Figure 16. Responses and control actions for Quenser DCMCT (13) during simulation.

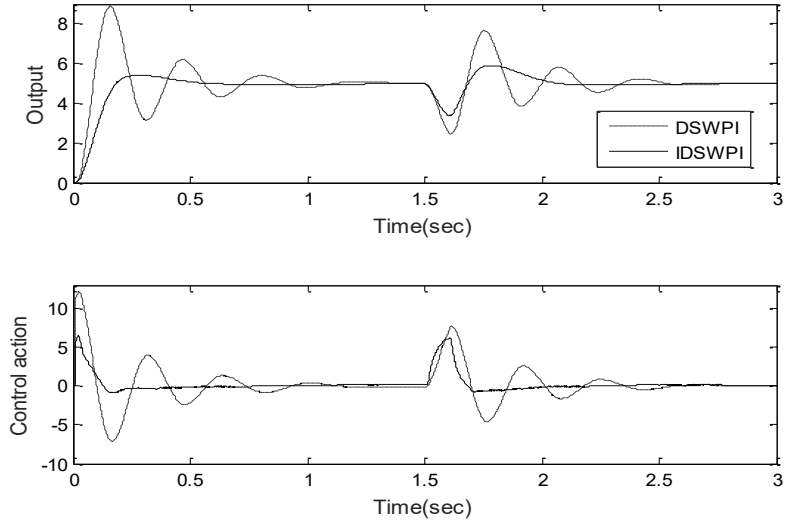

Figure 17. Responses and control actions for Quenser DCMCT (13) during real time experimentation.

Table 3 Performance analysis for DCMCT system in (13)

		%OS	t_r (sec)	t_s (sec)	IAE	ITAE	TV
FSWPI	simulation	67.1	0.3	5.0	1.22	3.67	0.29
DSWPI		81.1	0.3	4.0	1.14	3.04	0.28
IDSWPI		2.9	0.4	1.3	0.49	1.4	0.13
FSWPI	real time setup	Large oscillation present					
DSWPI		88.0	0.09	4.98	1.96	1.82	0.47
IDSWPI		40.0	0.18	0.67	0.99	0.78	0.16

International Journal of Environmental Sciences
ISSN: 2229-7359
Vol. 11 No. 6, 2025
https://theaspd.com/index.php

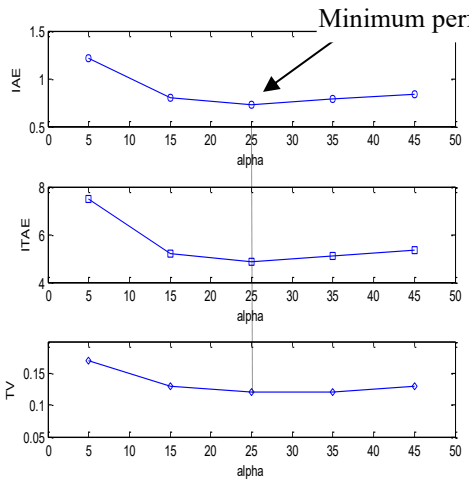

Figure 18. Variations of IAE, ITAE and TV values with α for QUBE servo system during simulation

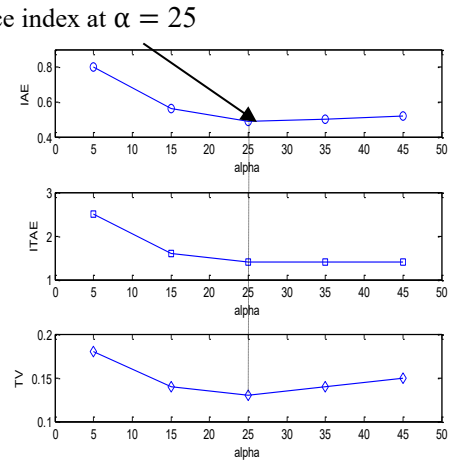

Figure 19. Variations of IAE, ITAE and TV values with α for DCMCT process during simulation

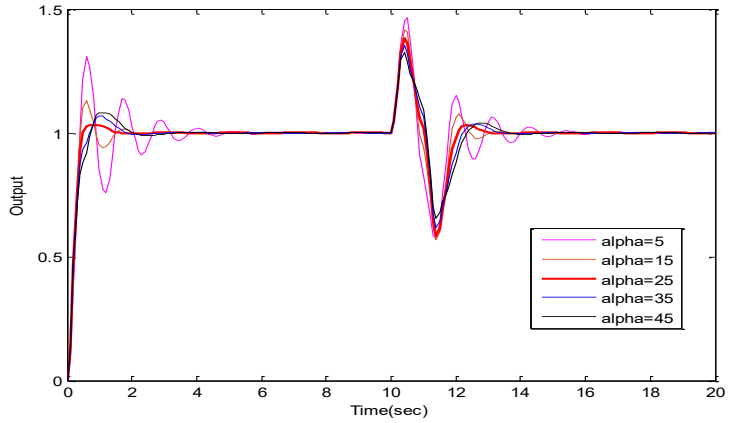

Figure 20. Closed loop responses with variations of slope parameter (α) for Qube servo during simulation

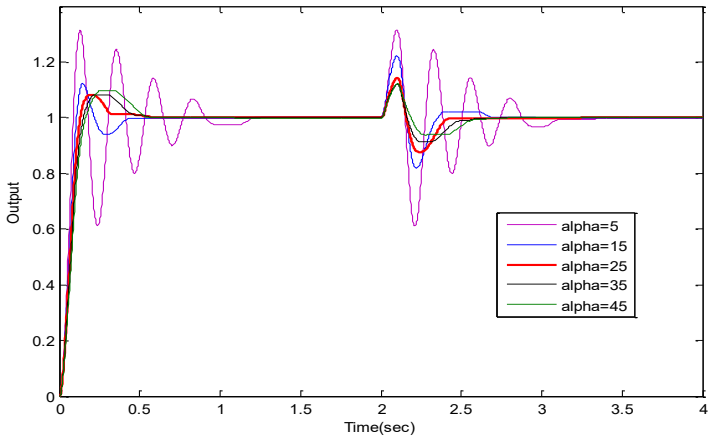

Figure 21. Closed loop responses with variations of slope parameter (α) for Qube servo during practical experimentation

International Journal of Environmental Sciences
ISSN: 2229-7359
Vol. 11 No. 6, 2025
https://theaspd.com/index.php

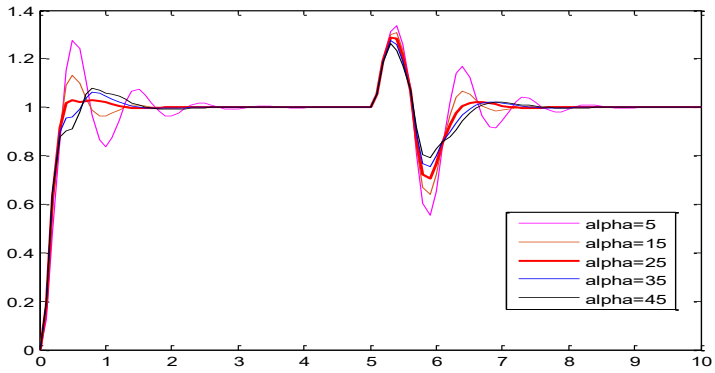

Figure 22. Closed loop responses with variations of slope parameter (α) for DCMCT process during simulation

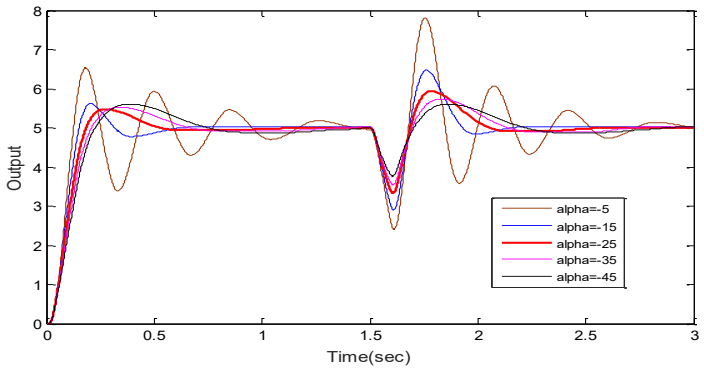

Figure 23. Closed loop responses with variations of slope parameter (α) for DCMCT process during practical experimentation

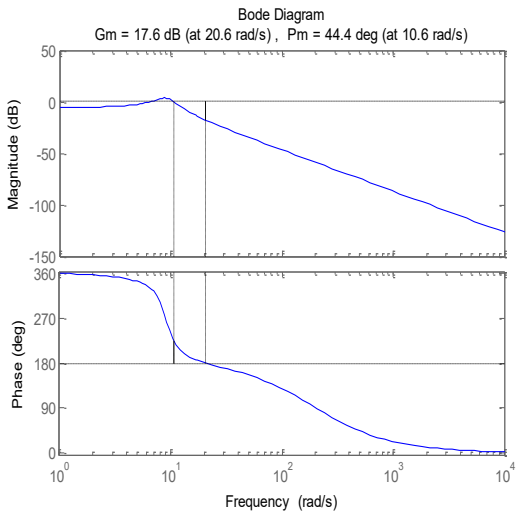

Figure 24. Stability margins for QUBE servo process in (12) at $\beta_{f\,max}$ [42]

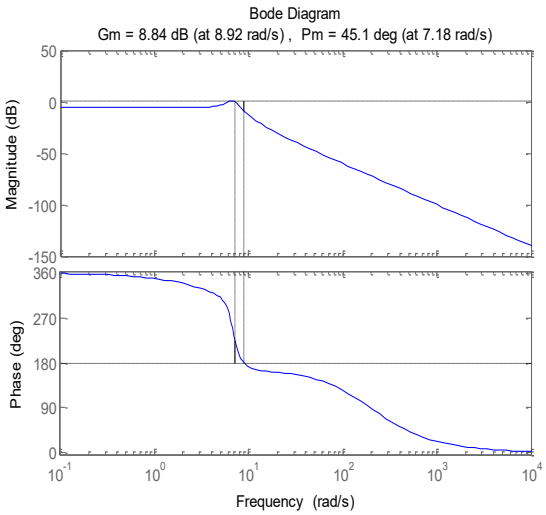

Figure 25. Stability margins for QUBE servo process in (12) at $\beta_{f\,min}$ [42]

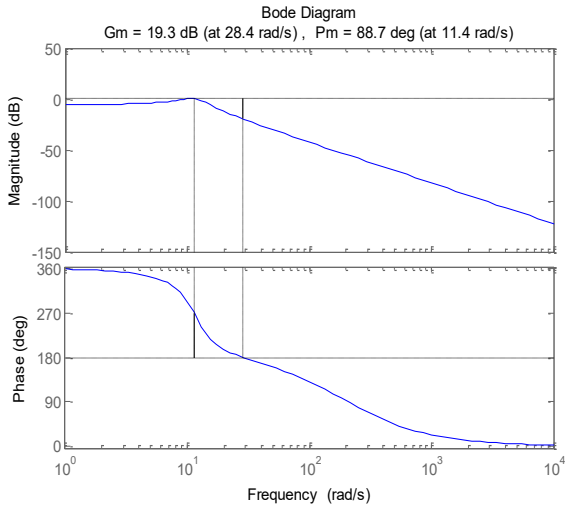

Figure 26. Stability margins for DCMCT process in (13) at $\beta_{f\,max}$ [43]

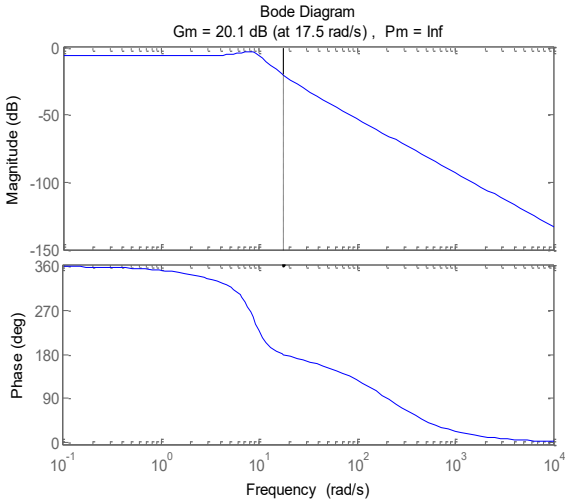

Figure 27. Stability margins for DCMCT process in (13) at $\beta_{f\,min}$ [43]

Table 4 Stability analysis of servo system

Model	Controller	Weighting factor (β_f)	Nominal Process		Maximum sensitivity (Ms)
			GM (dB)	PM (deg)	
QUBE Servo	FSWPI	$\beta_{f\,fixed}$	18.4 (19.5 rad/s)	48.5 (9.83 rad/s)	1.89
	DSWPI	$\beta_{f\,max}$	17.3 (20.8 rad/s)	43.4 (10.8 rad/s)	2.01
		$\beta_{f\,min}$	17.7 (20.5 rad/s)	44.7 (10.6 rad/s)	1.98
	IDSWPI	$\beta_{f\,max}$	17.6 (20.6 rad/s)	44.4 (10.6 rad/s)	1.98
		$\beta_{f\,min}$	8.84 (8.92 rad/s)	45.1 (7.18 rad/s)	1.85
DCMCT	FSWPI	$\beta_{f\,fixed}$	21.1 (26.6 rad/s)	Inf	1.47
	DSWPI	$\beta_{f\,max}$	18.4 (28.9 rad/s)	75.6 (12.7 rad/s)	1.61
		$\beta_{f\,min}$	19.3 (28.3 rad/s)	89.3 (11.4 rad/s)	1.56
	IDSWPI	$\beta_{f\,max}$	19.3 (28.4 rad/s)	88.7 (11.4 rad/s)	1.56
		$\beta_{f\,min}$	20.1 (17.5 rad/s)	Inf	1.41